Applied Energy 401 (2025) 126666

Contents lists available at ScienceDirect

Applied Energy

journal homepage: www.elsevier.com/locate/apen

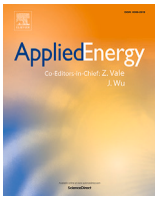

Experimental evaluation of model predictive control and fuzzy logic control for demand response in buildings

Felix Langner*, Jovana Kovačević, Luigi Spatafora, Stefan Dietze, Simon Waczowicz, Hüseyin K. Çakmak, Jörg Matthes, Veit Hagenmeyer

Karlsruhe Institute of Technology, Institute for Automation and Applied Informatics, Eggenstein-Leopoldshafen, Germany

HIGHLIGHTS

- Real-world comparison of advanced heating controls for building demand response.
- Three identical buildings enable a reliable control performance evaluation.
- Broad comparison includes various objectives, temperature bounds, and disturbances.
- CO2 and cost savings range from 2.1 % to 33.4 % while improving comfort.

ARTICLE INFO

Keywords:
Demand response
Fuzzy logic control
Model predictive control
Real experiment
Residential building

ABSTRACT

Energy flexibility is essential for aligning the energy demand with the intermittent electricity generation from renewable energy sources. In the European Union, buildings account for 40 % of the final energy consumption, thus offering significant potential for energy flexibility through load shifting, peak clipping, valley filling, and flexible load shaping. While experimental studies are crucial for providing realistic estimates of cost savings, comparing various control algorithms in the real world is inherently difficult. The present paper addresses this challenge by simultaneously controlling three architecturally identical buildings with different controllers to shift space heating in response to dynamic pricing. Model predictive control (MPC) and fuzzy logic control (FLC) are compared to a baseline control across various experiments, encompassing different objectives, price signals, and comfort levels. Over the course of a one-month experimental study, both MPC and FLC improved thermal comfort while achieving cost savings ranging from 7.8 % to 33.4 % and from 4.4 % to 8.6 %, respectively. The additional savings provided by MPC compared to FLC increase with greater price variability, indicating that MPC is particularly advantageous in markets with high price spreads. Conversely, when prices fluctuate less, the computationally more efficient FLC is sufficient. When minimizing costs, the MPC reduces the heating costs by 33.4 % but merely reduces the CO_2 emissions by 2.9 %. Consequently, focusing solely on cost minimization is insufficient to achieve substantial emission reductions.

1. Introduction

Buildings account for 26 % of global energy-related greenhouse gas emissions [1], making their decarbonization essential to achieving climate goals. In particular, space heating contributes to 66 % of energy consumption in buildings across the European Union [2], highlighting the necessity of decarbonizing the heating sector. One strategy to facilitate this transition is by extending district heating networks (DHNs) [3] to enable the integration of waste heat from, for instance, data centers and renewable energy resources [4].

In addition, electrifying the heat supply through heat pumps can also contribute to the decarbonization of the heating sector [5,6]. However, this requires that a large proportion of the electricity be generated from renewable energy sources. The main challenge of integrating renewable energies into the power grid is their volatile power generation, which can be addressed by integrating flexible loads into the energy system

* Corresponding author.
Email address: felix.langner@kit.edu (F. Langner).

https://doi.org/10.1016/j.apenergy.2025.126666
Received 16 April 2025; Received in revised form 23 July 2025; Accepted 20 August 2025
Available online 28 August 2025

Nomenclature

Acronyms

LLEC	Living Lab Energy Campus
BAU	Baseline-As-Usual
DHN	District Heating Network
DR	Demand Response
ECDF	Empirical Cumulative Distribution Function
FF	Flexibility Factor
FLC	Fuzzy Logic Control
HC	Heating Curve
MPC	Model Predictive Control
RBC	Rule-Based Control

Parameters

γ	Penalty for constraint violations
$\overline{T}_j$	Upper temperature bound in °C
$\underline{T}_j$	Lower temperature bound in °C
$C_{\mathrm{air},j}$	Heat capacity of the room air in J/K
$C_{\mathrm{h},j}$	Heat capacity of the floor in J/K
$C_{\mathrm{m},j}$	Heat capacity of the heat accumulating medium in J/K
f	Fraction of waste heat
g_j	Solar heat gain factor in m^2
N	Number of time steps in the prediction horizon
$R_{\mathrm{aa},j}$	Resistance between $T_{\mathrm{air},j}$ and T_{amb} in K/W
$R_{\mathrm{ah},j}$	Resistance between $T_{\mathrm{air},j}$ and $T_{\mathrm{h},j}$ in K/W
$R_{\mathrm{am},j}$	Resistance between $T_{\mathrm{air},j}$ and $T_{\mathrm{m},j}$ in K/W
t_s	Sample time in s

Subscripts

j	Room index
k	Time index

Variables

$\dot{Q}_{\mathrm{h},j}$	Emitted heat flow in W
$\dot{Q}_{\mathrm{sol}}$	Solar radiation in W/m^2
$\hat{F}$	Empirical cumulative distribution function
ξ	Slack variables for the MPC
p_{buy}	Heat price in ct/kWh
T^{set}	Temperature setpoint in °C
T_{supply}	Supply temperature in °C
T_{amb}	Ambient air temperature in °C
$T_{\mathrm{air},j}$	Indoor air temperature in °C
$T_{\mathrm{h},j}$	Floor temperature in °C
$T_{\mathrm{m},j}$	Heat accumulating medium temperature in °C
v_j	Valve opening

[7]. The “Heat Roadmap Europe” studies project that district heating could supply up to 50 % of the total heat demand of the EU27 states by 2050, with 25–30 % of it being supplied by large-scale heat pumps [8]. Therefore, DHNs will present a substantial potential for power flexibility. For the DHNs to provide power flexibility, incentives are required, which are provided by Demand Response (DR) programs. These programs encourage consumers to adjust their electricity consumption in response to dynamic prices [9]. For DHNs equipped with large-scale heat pumps to participate in a DR program and to provide power flexibly, heat flexibility is required to align the heat consumption with the heat pump’s operation. In contrast to power flexibility, heat flexibility refers to the ability to modify the heat demand instead of the electricity demand. The DHN operator can broadcast dynamic heat prices to incentivize the customers to shift their heat demand.

There are three different sources of heat flexibility in a DHN: (i) the circulating water in the network’s pipes, (ii) dedicated thermal energy storage, and (iii) the thermal mass of the buildings connected to the DHN. A limited amount of heat can be stored by increasing the temperature of the circulating water in the DHN. However, cycling between high and low temperatures may accelerate material fatigue and potentially result in pipe failure [10]. While storing heat in dedicated thermal energy storage is simple, constructing new storage capacities requires capital investment and suffers from heat losses. In contrast, the buildings connected to the DHN already exist and can be utilized for heat storage with limited costs for control installations [11]. Consequently, the present paper focuses on the heat flexibility of the buildings connected to the DHN. In particular, shifting the heat demand is incentivized through dynamic heat pricing. As control is the factor with the largest influence on buildings’ energy flexibility [12], this work contributes to answering the following research questions:

*RQ*1 Which control strategies unlock “energy flexibility” and to what extent?

*RQ*2 Is a simple control mechanism sufficient to achieve satisfactory control performance, or are advanced controls required?

1.1. Related work

Two main categories of controllers are widely investigated in literature for the control of building energy systems: rule-based control (RBC) and model predictive control (MPC) [13]. RBCs are explored for their simplicity and computational efficiency [13], resulting in enhanced robustness and facilitating easier implementation. Conversely, MPCs are examined for their superior performance and ability to directly consider constraints despite requiring substantial implementation effort [14].

Foteinaki et al. [11] investigate the application of an RBC to achieve load shifting in a building connected to district heating. Incentivized by dynamic heat pricing, indoor air temperature setpoints are increased or decreased, achieving cost savings of up to 15.5 %, compared to a baseline scenario with fixed setpoints. Clauß et al. [15] apply various RBC strategies to control an air-source heat pump providing space heating and hot water by modifying temperature setpoints. The controls minimize costs and reduce electricity consumption during peak hours with high electricity demand. While these controls successfully reduce electricity consumption during peak hours, they fail to reduce heating costs due to the limited variations in Norway’s dynamic electricity prices. In a field study, Mishra et al. [16] assess the demand response potential of a university building connected to district heating under dynamic heat pricing. By modifying supply temperature setpoints based on current and historical heat prices, they successfully shift loads to low-price periods without compromising occupant thermal satisfaction. However, the absence of energy consumption measurements prevents the assessment of potential cost savings.

Fuzzy logic control (FLC), an advanced variant of RBC, has received attention for coordinating building energy consumption in demand response events due to its capability of making reliable decisions with minimal information [17]. In the fuzzy logic approach, the input data are mapped into fuzzy membership values, and the decision is made by activating certain IF-THEN rules based on current input signals. The fuzziness allows for partial truth, with the solution taking values between zero and one, allowing for approximate reasoning as opposed to precise reasoning as in classical RBCs. Keshtkar et al. [17] utilize FLC for automated demand response, achieving energy consumption reductions during peak hours in response to dynamic electricity pricing. Similarly, Talebi and Hatami [18] evaluate achievable savings when controlling a building’s HVAC system with FLC, reporting 15 % cost savings from participating in a demand response program with dynamic pricing. Overall, RBCs demonstrate the potential for considerable benefits while retaining simplicity and computational efficiency. However, they cannot guarantee constraint satisfaction and lack the ability to

predict and anticipate [13], which has led to the exploration of MPC as an alternative approach.

Knudsen et al. [19] experimentally evaluate MPC for demand response in a residential building connected to district heating. Compared to a simulated baseline, the controller saves 22.5 % of costs under dynamic heat pricing. In a long-term experimental study, Thorsteinsson et al. [20] apply MPC for load shifting incentivized by dynamic electricity pricing in an occupied single-family house. Cost savings of 2–17 % are achieved compared to historical data from the previous year. In a simulation study, Hu et al. [21] employ MPC to control the underfloor heating system of a single room in a residential building. When considering dynamic pricing, the daily energy costs are reduced by 1.82–18.65 % while improving thermal comfort and reducing energy consumption during peak load times. Wei et al. [22] compare the achievable savings of MPC for two different building configurations: one with high thermal mass and one with low thermal mass. By shifting the heating loads to low-price periods, the controller saves 44.15 % and 13.58 % for the heavyweight and lightweight configurations, respectively. Similarly, Ramesh et al. [23] apply MPC to two buildings with different building envelope performance: a modern building and an older building. In two separate one-week simulations, the MPC achieves cost savings of up to 29.9 % for the older building and 14.8 % for the modern building, compared to a proportional-integral benchmark control. Wang et al. [24] develop a hierarchical nonlinear MPC for the price-responsive control of a residential inverter air conditioner. During a simulation of one cooling season, the MPC saves 14.3 % of electricity costs compared to the rule-based benchmark. In an experimental study, Morovat et al. [25] apply MPC to shift the electricity consumption of heat pumps in a school building in response to dynamic electricity pricing. Due to the substantial high-to-low electricity price ratio of 15, the MPC achieves 44 % electricity cost savings compared to the schedule-based reference. Hua et al. [26] combine FLC and MPC for demand response in an educational building that is heated by district heating and a heat pump. The controller achieves cost savings of 12.6 % by dynamically adjusting the indoor air temperature setpoints in response to the dynamic electricity price.

In summary, advanced building controls for demand response are widely researched, and promising results have been obtained. However, several gaps in the available literature have been identified.

1.2. Research gaps and contributions

1.2.1. Lack of real-world implementations

While the advantages of advanced control have been demonstrated extensively through simulations, the limited number of real-world implementations hinders widespread adoption [13,27]. The present paper contributes by presenting experimental results, illustrating the benefits of advanced control for demand response in buildings.

While it is common to present the benefits of advanced control algorithms, the deployment efforts and costs are rarely discussed [28]. This has been identified as a substantial impediment to the widespread application of advanced control algorithms [27,29]. The present work contributes by disclosing the deployment efforts and costs.

1.2.2. Lack of reliable comparisons

Comparing different control algorithms is non-trivial, as buildings are subject to uncontrollable factors such as weather and occupant behavior [20], which precludes the repetition of experiments under identical conditions. Seemingly, this obstacle appears to be solved by resorting to simulations or by controlling similar rooms inside a building. However, Pergantis et al. [28] stress that both simulations and controlling only a subset of a building tend to overestimate the achievable savings. The present work addresses this challenge by controlling three architecturally identical buildings subject to almost identical weather and occupancy conditions, facilitated by the unique infrastructure of the Living Lab Energy Campus (LLEC) as part of the Energy Lab [30,31] at Karlsruhe Institute of Technology. The issue of integrating identical occupant behavior is managed by conducting experiments without occupants, thus enabling an accurate comparison of controller performance. However, during phases of the experiments, occupant behavior is mimicked by leveraging the fully automated infrastructure of the LLEC to simultaneously operate the corresponding windows, roller shutters, and doors across all three buildings.

1.2.3. Lack of broad comparisons

Most works in existing literature evaluate the performance improvement of one particular application over a benchmark instead of assessing a range of methods [29]. However, when developing an advanced controller such as MPC, comparison with a single baseline may prove insufficient. This is particularly relevant given that a much simpler controller could realize a significant proportion of the savings achieved by MPC. Specifically, Thorsteinsson et al. [20] observed that, in their experiment, 66 % of the savings achieved by MPC could be accomplished by simply blocking heat generation during the evening price peak. Therefore, evaluating whether a simpler controller could obtain the majority of benefits is essential. However, due to the inherent difficulties of comparing controllers in real experiments, advanced controllers are typically benchmarked by either simulating a baseline controller (e.g., [19]) or alternating the application of the advanced and baseline controls (e.g., [32]). The present paper contributes by evaluating both MPC as an optimization-based control and FLC as a rule-based control, thereby enabling an estimation of whether the increased complexity of MPC over FLC is justified. Furthermore, the controls are compared in multiple experiments with different price signals, thermal comfort requirements, and disturbances, thereby evaluating the controls in various settings. The dataset accompanying the present work can be found in [33].

1.3. Structure of the present paper

The remainder of this paper is organized as follows. The experimental buildings are presented first in Section 2. Subsequently, MPC and FLC are introduced in Section 3. The case study used to compare the performance of the controllers is described in Section 4. The results are presented and discussed in Section 5. The paper is concluded in Section 6 with a discussion and an outlook for future work.

2. Experimental buildings

The experiments are conducted in three buildings of the Living Lab Energy Campus at Karlsruhe Institute of Technology (see Fig. 1a). The buildings are constructed as architecturally identical two-story residential buildings with a living area of approximately 100 m^2, comprising five rooms, a kitchen, and a bathroom. The buildings' layout is provided in Fig. 1b.

Since the utility rooms are not accessible from the inside of the buildings and are only used to configure the buildings' hydraulics, they are neglected in the remainder. The buildings are constructed in accordance with the EnEV 2016 standard [34]. Accordingly, the buildings' envelopes consist of aerated concrete with a thickness of 0.36 m and a design U-value of 0.23 $W/(m^2K)$. The roofs, constructed from sandwich panels, are designed with a U-value of 0.18 $W/(m^2K)$. The flooring comprises 0.25 m of reinforced concrete topped with a 0.1 m layer of Styrodur insulation and 5 cm of screed in which the underfloor heating pipes are embedded. The approximate ratios of windows to walls for the north, east, south, and west facades are 20 %, 3.5 %, 35 %, and 13 %, respectively. The buildings are connected to the Karlsruhe Institute of Technology campus's district heating and distribute the heat via an underfloor heating system. Fig. 2 presents the hydraulic layout.

Each building receives the same supply temperature of the district heating network $T_{\text{supply}}^{\text{DHN}}$ which is mixed with the return water of the underfloor heating system T_{return} to reach the desired temperature setpoint. A pump distributes the mixed water with the supply temperature T_{supply} into each of the J rooms. Each room is equipped with a valve to

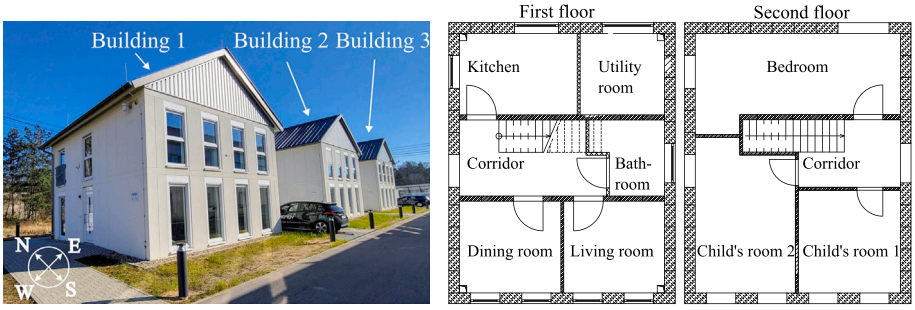

(a) The three experimental buildings. (b) The layout of the experimental buildings.

Fig. 1. The experimental buildings at LLEC at Karlsruhe Institute of Technology.

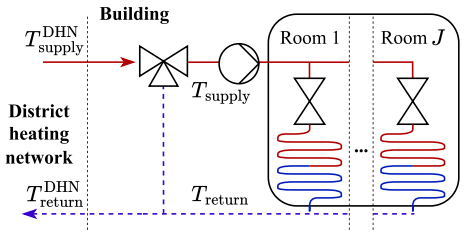

Fig. 2. Simplified hydraulic setup of each building. Solid lines represent the supply pipes and dashed lines the return pipes.

control the mass flow of the supply water. The buildings are equipped with wall-mounted indoor air temperature sensors and heat flow meters to measure the underfloor heating system's mass flows, supply temperatures, and return temperatures of each heating circuit at a room level. The indoor air temperature sensors are mounted at a height of 1.4 m.

Fig. 3 illustrates the communication flow within the experimental buildings.

The controllers are implemented in Python and run on stationary computers. They access locally stored price data (p_{buy}) and retrieve forecasts for the ambient air temperature (T_{amb}) and the solar radiation ($\dot{Q}_{\text{sol}}$) from the German Weather Service [35] via an application programming interface [36]. Additionally, they read real-time measurements of indoor air temperatures (T_{air}) from InfluxDB. Utilizing this information, the controllers (details in Section 3) calculate setpoints for both indoor air temperatures ($T^{\text{set}}_{\text{air}}$) and the supply temperature of the underfloor heating system ($T^{\text{set}}_{\text{supply}}$). These setpoints are communicated via MQTT to a Programmable Logic Controller (PLC). The PLC then relays the indoor air temperature setpoints to the room thermostats and the supply temperature setpoint to the mixing valve (see Fig. 2). Local controllers (details in Section 3) track the temperature setpoints by adjusting valve openings v. Furthermore, the PLC continuously monitors and communicates the supply temperature and indoor air temperature measurements, which are stored in InfluxDB through MQTT.

3. Controls

Two sets are introduced for notational brevity: $\mathcal{J} = \{R1, R2, R3, R4, R5, K, B, C\}$ is a set containing all rooms and $\mathcal{K} = \{1, 2, \dots, N\}$ contains the natural numbers from 1 to N, where N is the number of time steps in the MPC's prediction horizon. As the MPC utilizes a sample time of $t_s = 15$ min and a prediction horizon of 24 h, N equals 96 time steps. The indices j and k denote the room and time index, respectively.

Three controls are compared: baseline-as-usual (BAU), FLC, and MPC. All controllers are designed as supervisory controls, which write setpoints that are tracked by local controllers. This facilitates the transferability of the developed approaches to other buildings using different local controllers. The supervisory controllers determine two types of setpoints: (i) setpoints of the indoor air temperature for each of the eight rooms $T^{\text{set}}_{\text{air},j}$ and (ii) one setpoint for the supply temperature of the underfloor heating system's heating manifold $T^{\text{set}}_{\text{supply}}$. The local controllers tracking these setpoints are on/off controllers and PI controllers for the room and supply temperature setpoints, respectively. Fig. 4 visualizes the control architecture.

The three controllers, BAU, FLC, and MPC, differ in the information they require. While BAU only requires information about the current ambient air temperature, FLC also needs information about the future dynamic prices, and MPC additionally requires the weather forecast. The controllers aim to minimize heating costs while maintaining comfortable indoor air temperatures. The comfortable range of the indoor air temperature is indicated by room-individual and time-varying lower ($\underline{T}_{j,k}$) and upper ($\overline{T}_{j,k}$) temperature bounds.

3.1. Baseline-as-usual control

The baseline controller aims to minimize heating energy without considering the energy prices. The supply temperature setpoint of the underfloor heating system is determined based on the ambient air temperature according to the heating curve (HC) presented in Fig. 5.

The variable $T_{\text{supply,HC}}$ indicates the supply temperature according to the heating curve. The supply temperature setpoint is selected as

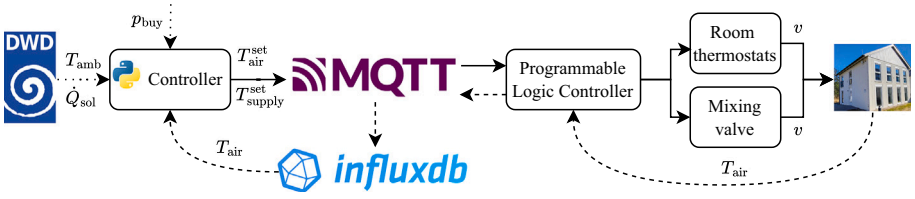

Fig. 3. Overview of the communication flow in the buildings. Dotted lines represent external forecasts, solid lines represent control actions, and dashed lines represent measurements.

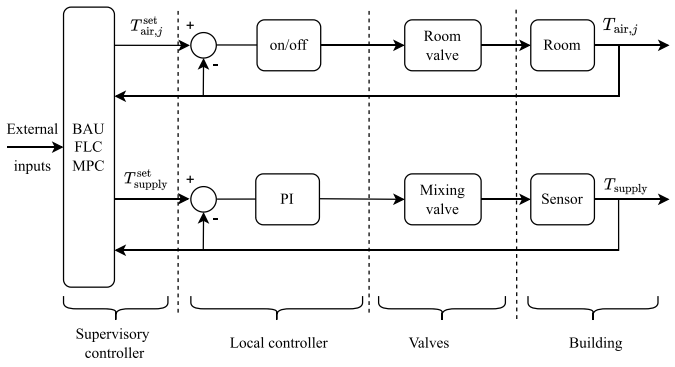

Fig. 4. The supervisory control architecture of the examined controllers BAU, FLC, and MPC.

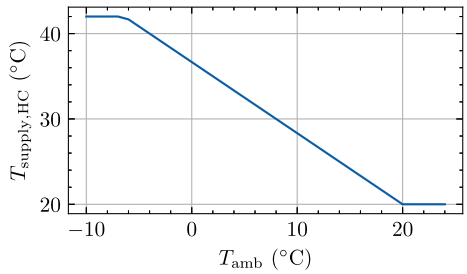

Fig. 5. The heating curve for BAU.

$T^{set}_{supply,k} = T_{supply,HC,k}$. The room temperature setpoints are selected as the lower acceptable temperature bounds (i.e., $T^{set}_{air,j,k} = \underline{T}_{j,k}$) to ensure minimal energy consumption.

3.2. Fuzzy logic control

As outputs, the FLC determines room temperature setpoints $T^{set}_{air,j,k+1}$ and a supply temperature setpoint for the underfloor heating system $T^{set}_{supply,k+1}$ for the following time step (i.e., $k+1$). While the room temperature setpoints are determined directly, the supply temperature setpoint is selected by calculating a temperature offset (ΔT_{supply}) to the existing heating curve (see Fig. 5). The FLC makes decisions for each room j based on four inputs:

1. The difference between the lower temperature bound and the indoor air temperature e_j to avoid underheating (Eq. (1a)).
2. The change in room temperature $\Delta T_{air,j}$ within one time step, which indicates the appearance of disturbances (Eq. (1b)). For instance, a rapidly dropping indoor air temperature can indicate open windows.
3. The change of the lower temperature bound within the following six hours Δo_j (Eq. (1c)). This allows the controller sufficient time to preheat the room, if necessary, or to decrease the heating if the room is not expected to be occupied in the following period. Six hours are selected as the underfloor heating system is very inert. A time horizon of six hours equals 24 time steps, which also equals $N/4$ as a sample time of 15 min is used.
4. The Empirical Cumulative Distribution Function (ECDF) of the day-ahead heat price $\hat{F}\left(p_{buy}\right)$ to indicate if the price is currently low or high relative to the future prices.

$$e_{j,k} = \underline{T}_{j,k} - T_{air,j,k} \tag{1a}$$

$$\Delta T_{air,j,k} = T_{air,j,k} - T_{air,j,k-1} \tag{1b}$$

Table 1
The part of the rule base is defined according to $\underline{T}_{j,k}$. The abbreviations stand for: `Z` – `Zero`, `SP` – `Small Positive`, `MP` – `Medium Positive`, `BP` – `Big Positive`, `LB` – `Lower Bound`. *All* includes all possible cases.

$\underline{T}_{j,k}$	Rule no.	$e_{j,k}$	$\Delta T_{air,j,k}$	$\Delta o_{j,k}$	$\hat{F}(p_{buy})_k$	$T^{set}_{air,j,k+1}$	$\Delta T_{supply,j,k+1}$
21 °C	1	Zero	Zero	Zero	Low	T_{SP}	SP
	2	Zero	Zero	Zero	Avg./High	T_{LB}	Z
	3	Zero	Colder	Zero	Low	T_{BP}	BP
	4	Zero	Colder	Zero	High	T_{LB}	SP
	5	Zero	Warmer	Zero	All	T_{LB}	Z
	6	Zero	Zero	Colder	All	T_{LB}	Z
	7	Zero	Colder	Colder	Low	T_{BP}	BP
	8	Zero	Colder	Colder	Avg.	T_{MP}	MP
	9	Warm	Zero	All	All	T_{LB}	Z
	10	Cold	All	All	All	T_{LB}	BP
18 °C	11	Zero	Zero	Warmer	Low	T_{SP}	SP
	12	Zero	Zero	Warmer	Avg./High	T_{LB}	Z
	13	Zero	Colder	Warmer	Low	T_{MP}	BP
	14	Zero	Colder	Warmer	Avg.	T_{SP}	MP
	15	Zero	All	Zero/Colder	All	T_{off}	Z
	16	Hot/Cold	All	Zero/Colder	All	T_{off}	Z
	17	Warm	Zero	Warmer	Low	T_{SP}	SP

$$\Delta o_{j,k} = \underline{T}_{j,k} - \underline{T}_{N/4,j,k} \tag{1c}$$

$$\underline{T}_{N/4,j,k} = \begin{cases} \underline{T}_{j,k+w}, \text{ if } \exists w : \underline{T}_{j,k+w-1} \neq \underline{T}_{j,k+w} \text{ for } w \in \{1, 2 \dots N/4\} \\ \underline{T}_{j,k+N/4}, \text{ otherwise} \end{cases} \tag{1d}$$

Detailed information about the membership functions is given in Appendix A. Based on the current input information, the controller determines the next room temperature setpoint and the normalized increment for the supply temperature $\Delta T_{supply,j,k+1}$ for each room independently. The maximum increment is selected to ensure that each room receives sufficient heat, multiplied by α and added to the baseline supply temperature $T_{supply,HC}$, as indicated in Eq. (2).

$$T^{set}_{supply,k+1} = T_{supply,HC,k} + \alpha \cdot \max_j \left(\Delta T_{supply,j,k+1}\right); \quad \alpha = 10 \tag{2}$$

As the lower temperature bounds $\underline{T}$ differ between 18 °C and 21 °C (see Table 3), two sets of rules are created. Table 1 provides an overview of the rules for both cases.

For example, if a high heat demand is detected and the heat price is low simultaneously, the FLC decides to heat the building strongly. This configuration occurs for instance, if the temperature difference $e_{j,k}$, for room j at time step k is `Zero`, a dropping indoor air temperature is detected (i.e., $\Delta T_{air,j,k}$ is `Colder`), no change in the lower temperature bound occurs in the next 6 hours, (i.e., $\Delta o_{j,k}$ is `Zero`), and the heat price's ECDF $\hat{F}(p_{buy})_k$ is `Low`, then the room temperature setpoint of the following time step $T^{set}_{air,j,k+1}$ is T_{BP}, indicating significant heating. Moreover, the controller proposes to increase the supply temperature $\Delta T_{supply,j,k+1}$, returning an increment described as `Big Positive` – `BP`. Conversely, the controller avoids strong heating if the price signal $\hat{F}(p_{buy})_k$ is `High` while the rest of the inputs remain unchanged. In particular, the room temperature setpoint is set to the lower temperature bound, while the supply temperature is slightly increased (`Small Positive`) to counteract the dropping temperature.

3.3. Model predictive control

The MPC utilizes a grey-box multi-zone model, where the thermal dynamics of each room j are modeled as a third-order resistance-capacitance model with capacitances for the indoor air (C_{air}), thermal mass (C_m), and the floor (C_h).

$$C_{\mathrm{air},j}\frac{dT_{\mathrm{air},j}}{dt} = \frac{T_{\mathrm{m},j}-T_{\mathrm{air},j}}{R_{\mathrm{am},j}} + \frac{T_{\mathrm{amb}}-T_{\mathrm{air},j}}{R_{\mathrm{aa},j}} + \frac{T_{\mathrm{h},j}-T_{\mathrm{air},j}}{R_{\mathrm{ah},j}} + g_j\cdot\dot{Q}_{\mathrm{sol}} \quad \forall j\in\mathcal{J} \tag{3a}$$

$$C_{\mathrm{m},j}\frac{dT_{\mathrm{m},j}}{dt} = \frac{T_{\mathrm{air},j}-T_{\mathrm{m},j}}{R_{\mathrm{am},j}} \quad \forall j\in\mathcal{J} \tag{3b}$$

$$C_{\mathrm{h},j}\frac{dT_{\mathrm{h},j}}{dt} = \frac{T_{\mathrm{air},j}-T_{\mathrm{h},j}}{R_{\mathrm{ah},j}} + \dot{Q}_{\mathrm{h},j} \quad \forall j\in\mathcal{J}\setminus\{K,C\} \tag{3c}$$

The indoor air, thermal mass, and floor exchange heat via thermal resistances R. The influence of the solar radiation $\dot{Q}_{\mathrm{sol}}$ and the ambient air temperature T_{amb} on the indoor air temperature is captured in Eq. (3a), where the solar radiation is multiplied by a room-specific solar heat gain factor g_j, to account for varying window sizes. The floor is heated with the heat flow $\dot{Q}_{\mathrm{h}}$ transferred by the supply water of the underfloor heating system.

The heating pipes in the screed transport the hot supply water to the rooms. Each of the pipes has to cross the kitchen and the corridor until they reach their destination. Therefore, the kitchen and the corridor receive substantial waste heat, which is not captured in Eq. (3c). Consequently, Eq. (3c) is replaced in the models for the corridor and kitchen with

$$C_{\mathrm{h},j}\frac{dT_{\mathrm{h},j}}{dt} = \frac{T_{\mathrm{air},j}-T_{\mathrm{h},j}}{R_{\mathrm{ah},j}} + \dot{Q}_{\mathrm{h},j} + \sum_{n\in\mathcal{J}\setminus\{K,C\}} f_{j,n}\dot{Q}_{\mathrm{h},n} \quad \forall j\in\{K,C\} \tag{4}$$

where, e.g., $f_{K,R1}$ is an identifiable parameter representing the fraction of waste heat flowing into the kitchen if the room $R1$ is heated. The Eqs. (3a)-(4) can be reformulated into a time-discrete state-space system using a zero-order hold discretization according to

$$\mathbf{x}_{k+1} = \mathbf{A}\mathbf{x}_k + \mathbf{B}\mathbf{u}_k \tag{5a}$$

$$\mathbf{y}_k = \mathbf{C}\mathbf{x}_k \tag{5b}$$

where the state vector $\mathbf{x} = [T_{\mathrm{air},R1}, T_{\mathrm{m},R1}, T_{\mathrm{h},R1}, \dots, T_{\mathrm{h},C}]^\top$ contains the temperatures of each room model, the output vector $\mathbf{y} = [T_{\mathrm{air},R1}, \dots, T_{\mathrm{air},C}]^\top$ represents the indoor air temperatures of each room, and the input vector $\mathbf{u} = [\dot{Q}_{\mathrm{h},R1}, \dots, \dot{Q}_{\mathrm{h},C}, T_{\mathrm{amb}}, \dot{Q}_{\mathrm{sol}}]^\top$ contains the heat flows supplied to the underfloor heating system in each room and the weather conditions. k denotes the time step. The parameters R, C, g, and f are optimized based on measurement data. Details are provided in Appendix B.

While the resistance-capacitance model uses the heat flows $\dot{Q}_{\mathrm{h}}$ as input, the MPC can only indirectly influence $\dot{Q}_{\mathrm{h}}$ by setting temperature setpoints for the lower level controllers, which control the valve openings and thereby the supply temperature and the indoor air temperatures. Therefore, the heat flows $\dot{Q}_{\mathrm{h}}$ have to be mapped to temperature setpoints. The knowledge that the lower level controller monitoring the room temperatures either fully opens or closes the valves (see Fig. 4) can be leveraged by introducing

$$\upsilon_j \in \{0,1\} \quad \forall j\in\mathcal{J} \tag{6}$$

where the binary variable υ_j describes if the valve in room j is closed ($\upsilon_j = 0$) or open ($\upsilon_j = 1$). Since no heat flow is emitted when the valve is closed, the required mapping can be expressed as

$$\dot{Q}_{\mathrm{h},j} = \begin{cases} 0, & \text{if } \upsilon_j = 0 \\ m_j(T_{\mathrm{supply}}), & \text{if } \upsilon_j = 1 \end{cases} \tag{7}$$

where m_j is a function that maps the supply temperature to the emitted heat flow for each room j. Selecting m_j as linear functions was found to be sufficiently accurate while enabling a quick optimization. Detailed information about the data collection, model identification, and model validation results for the thermal building model and m_j can be found in Appendix B.

The model predictive controller is formulated as

$$\min_{\upsilon, T_{\mathrm{supply}}} \left(\sum_{k\in\mathcal{K}}\sum_{j\in\mathcal{J}} \left(p_{\mathrm{buy},k}\cdot\dot{Q}_{\mathrm{h},j,k} + \gamma\cdot|\xi_{j,k}|_2 \right) \right) \tag{8}$$

subject to

equations (5a) – (7)

$$\underline{T}_{j,k} - \xi_{j,k} \le T_{\mathrm{air},j,k} \le \overline{T}_{j,k} + \xi_{j,k} \quad \forall k\in\mathcal{K}, \forall j\in\mathcal{J} \tag{9}$$

where the objective function Eq. (8) minimizes the heating cost and penalizes violations of the constraint Eq. (9). The non-negative slack variables ξ are required to guarantee the feasibility of the optimization problem if the constraint (9) cannot be satisfied. For a sufficiently high value of γ, this forces the MPC to maintain the indoor air temperatures within comfortable bounds, characterized by minimum ($\underline{T}$) and maximum permitted temperatures ($\overline{T}$). In a post-processing step, a valve opening of $\upsilon = 0$ is mapped to a setpoint of the room thermostat of $T^{\mathrm{set}}_{\mathrm{air}} = 18$ °C and $\upsilon = 1$ is mapped to $T^{\mathrm{set}}_{\mathrm{air}} = 24$ °C, as 18 °C and 24 °C are the lowest and highest temperature bounds throughout the experiments (see Section 4). The supply temperature setpoint is set to the supply temperature as optimized by the MPC (i.e., $T^{\mathrm{set}}_{\mathrm{supply}} = T_{\mathrm{supply}}$).

4. Case study

The experiment aimed to investigate the performance of FLC and MPC under various conditions. The experiment was conducted over a four-week period from Dec. 22, 2024, to Jan. 19, 2025, and from Feb. 14 to 16, 2025, encompassing five different experiments. The experiments differ with respect to their objectives, price signals, permitted ranges for indoor air temperatures, and disturbances. In addition, a period called “Energy comparison” was conducted to ensure that the buildings behaved sufficiently similarly for a valid comparison. Table 2 provides an overview of the experimental schedule.

To minimize differences between the buildings, all interior doors are closed in each building, and all electrical devices (such as computers) are turned off. During experiments 1, 2, 3, and 5, the roller shutters of the west facade for the western building and the east facade for the eastern building are closed to minimize solar radiation gains that the central building does not receive. Conversely, during experiment 4, the roller shutters are opened to allow for ventilation during window operation.

4.1. Objectives and price signals

As objectives, cost minimization and CO_2 minimization are considered. In contrast to dynamic electricity prices, dynamic heat prices are

Table 2
The experimental schedule. “Bounds” refers to the lower and upper bounds for the indoor air temperature.

	Dates	Objective	Varying bounds	Disturbed	Price signal	Days
Experiment 1	Dec. 22 – 28	Cost minimization	No	No	Variable	1 – 7
Experiment 2	Dec. 30 – Jan. 05	Cost minimization	Yes	No	Variable	1 – 7
Experiment 3	Feb. 14 – 16	Cost minimization	Yes	No	Variable + constant	4 – 6
Experiment 4	Jan. 10 – 12	Cost minimization	Yes	Yes	Variable + constant	4 – 6
Experiment 5	Jan. 15 – 19	CO_2 minimization	No	No	—	3 – 6
Energy comparison	Jan. 6 – 9	—	—	—	—	—

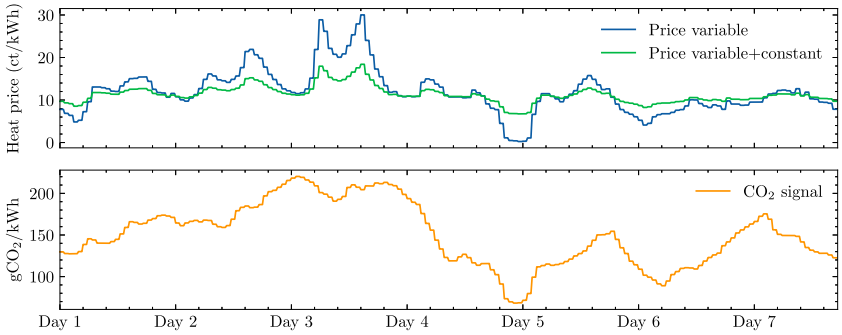

Fig. 6. The price and CO_2 signals used throughout the experiments.

not yet established. Therefore, electricity spot prices are selected as the basis for the price signals, even though the buildings are connected to a DHN. The week from Dec. 2 to Dec. 8, 2024 is selected as it includes days with large and minor fluctuations in the electricity price.

Two distinct price signals are evaluated: "variable" and "variable + constant". The price signal "variable + constant" is derived from a currently available tariff in Germany provided by tado [37], wherein a substantial portion of the electricity price is fixed to account for grid charges and taxes, while only a part of the electricity price varies according to the spot market price. However, recent legislation in Germany stipulates that starting from April 2025, grid charges can also vary throughout the day [38]. Specifically, the charges are lower during times of low demand and higher during peak times to incentivize load shifting. Consequently, the price signal "variable", only consists of the spot market price to assess the effect of a fully dynamic pricing scheme. Both price signals are rescaled such that the average price equals the current price of the district heat in Karlsruhe, Germany, obtained from Ref. [39].

The CO_2 signal is derived by calculating the emissions based on the operating power plants retrieved from the German federal grid agency [40] and their corresponding CO_2 emission factors, obtained from IPCC [41]. To calculate the CO_2 emissions per kWh heat, rather than per kWh electricity, the signal is divided by 2.7, representing the coefficient of performance of the large-scale heat pump supplying the DHN in Mannheim, Germany [42]. Fig. 6 presents the price and CO_2 signals. The column "Days" in Table 2 indicates which section of the price signals was applied during the respective experiments.

4.2. Temperature bounds

Two configurations of the allowable temperature bounds are used in the experiments. First, the lower and upper temperature bounds for all rooms are consistently set at 21 °C and 24 °C, respectively. This configuration clearly separates the controllers' preheating due to low energy prices from preheating because the controllers anticipate an increase in the lower temperature bound.

In the second configuration, room-individual and time-variant temperature bounds are applied to each room based on their intended use (e.g., bedroom, kitchen). For this purpose, an occupancy schedule is retrieved from Ref. [43], distinguishing occupant presence between "home", "away", and "sleep", and differentiating between weekends and weekdays. Table 3 presents the lower and upper temperature bounds for each room and occupant presence, and Table 4 details the schedule for the occupancy presence.

4.3. Disturbances

Introducing identical disturbances to emulate occupancy while still ensuring comparability between the three buildings is achieved by utilizing the fully automated infrastructure of the experimental buildings. The windows are opened in the morning and evening to ventilate the rooms. At night, the roller shutters are automatically lowered, and the internal doors are securely closed. In the morning, the internal doors are opened and the roller shutters are raised. The internal doors remain open throughout the day to increase the difference from the other experiments in which the doors are closed. A detailed timeline of the introduced disturbances is provided in Appendix C.

Table 3
Room use and associated temperature constraints.

Abbreviation	Room	$\underline{T}/\overline{T}$: sleep	$\underline{T}/\overline{T}$: home	$\underline{T}/\overline{T}$: away
R1	Dining room	18/24 °C	21/24 °C	18/24 °C
R2	Living room	18/24 °C	21/24 °C	18/24 °C
R3	Children's room 1	18/22 °C	21/24 °C	18/24 °C
R4	Children's room 2	18/22 °C	21/24 °C	18/24 °C
R5	Bedroom	18/22 °C	18/24 °C	18/24 °C
K	Kitchen	18/24 °C	21/24 °C	18/24 °C
B	Bathroom	18/24 °C	21/24 °C	18/24 °C
C	Corridor	18/24 °C	18/24 °C	18/24 °C

Table 4
Schedule for the occupancy presence.

	Home	Sleep	Away
Weekday	6–8 am, 5–11 pm	11 pm–6 am	8 am–5 pm
Weekend	6 am–11 pm	11 pm–6 am	–

4.4. Evaluation metrics

The control performance is evaluated using three metrics: energy cost c_{energy}, Flexibility Factor FF, and daily room-average thermal discomfort d. The discomfort has to be considered to ensure that the controllers do not achieve low costs by insufficiently heating the buildings. The FF has been proposed by Ref. [44] and describes the ability of the controller to shift the heat consumption from times with high prices to times with low prices. The factor ranges from -1 (i.e., only heating in high-price periods) to 1 (i.e., only heating in low-price periods). In this work, the FF is evaluated for each individual day, and prices in the first and fourth quartiles are considered as "low" and "high" based on [44]. If the controller heats equally during low and high price periods, then $FF = 0$. The metrics are calculated as

$$c_{\text{energy}} = t_{\text{s}} \cdot \sum_{k \in \mathcal{K}} \sum_{j \in J} p_{\text{buy},k} \cdot \dot{Q}_{\text{h},j,k} \tag{10}$$

$$FF = \frac{\sum_{k \in \mathcal{K}_{\text{low}}} \dot{Q}_{\text{h},k} - \sum_{k \in \mathcal{K}_{\text{high}}} \dot{Q}_{\text{h},k}}{\sum_{k \in \mathcal{K}_{\text{low}}} \dot{Q}_{\text{h},k} + \sum_{k \in \mathcal{K}_{\text{high}}} \dot{Q}_{\text{h},k}} \tag{11}$$

$$d = \frac{1}{J \cdot N} \cdot t_{\text{s}} \cdot \sum_{j=1}^{J} \sum_{k=1}^{M} d_{j,k} \tag{12}$$

Table 5
Energy consumption during the experiment "Energy comparison" from Jan. 06 – 09.

	Energy consumption	Difference	Orientation	Control
Building 1	129.3 kWh	—	West	BAU
Building 2	129.7 kWh	+0.3 %	Center	MPC
Building 3	122.7 kWh	−5.1 %	East	FLC

$$d_{j,k} = \begin{cases} \underline{T}_{j,k} - T_{\mathrm{air},j,k} & \text{if} \quad T_{\mathrm{air},j,k} < \underline{T}_{j,k} \\ T_{\mathrm{air},j,k} - \overline{T}_{j,k} & \text{if} \quad T_{\mathrm{air},j,k} > \overline{T}_{j,k} \\ 0 & \text{else} \end{cases} \tag{13}$$

where t_s is the sample time. The energy cost c_{energy} is calculated as the sum of the room-individual heat consumption multiplied by the current heat price. For the calculation of the FF, time steps with low and high prices are contained in the sets $\mathcal{K}_{\mathrm{low}}$ and $\mathcal{K}_{\mathrm{high}}$, respectively. The heat flow $\dot{Q}_{\mathrm{h},k}$ is the total heat flow utilized by the building. When minimizing CO_2 emissions, the FF is applied analogously, except that the price signal is replaced with the CO_2 signal. The daily room-average thermal discomfort d is calculated as the magnitude of the temperature bound violation in each room times the duration of the violation. M refers to the number of time steps in the respective experiment, N is the number of time steps in a day, and J is the number of rooms.

5. Results and discussion

For a reliable performance evaluation, it is essential that the three buildings behave sufficiently similarly. This was examined in the experiment "Energy comparison" (see Table 2), in which each building received identical supply temperature and room temperature setpoints of 40 °C and 21 °C, respectively. Table 5 presents the resulting energy consumption of each building. For a visualization of the buildings, please refer to Fig. 1a.

Notably, Buildings 1 and 2 consumed almost identical energy quantities. However, Building 3 consumed 5.1 % less energy despite being architecturally identical. Presumably, this is caused by wind effects, as this period was characterized by heavy southwest and west winds. Due to the orientation of the buildings, this predominantly affects Building 1, which wind-shadows Building 2, but both of these buildings, in turn, wind-shadow Building 3. This hypothesis is supported by data collected from Dec. 25 and Jan. 16–17, during which only minimal wind occurred, and all three controllers applied very similar control actions. During these periods, the differences in energy consumption among the three buildings remained below 1 %, supporting the hypothesis that wind conditions caused the discrepancies. Given that the wind speeds during the experiments 1–5 were significantly lower than in the experiment "Energy comparison", the buildings are considered to behave sufficiently similarly. Detailed time series data of wind speed and wind direction can be found in Appendix D.

5.1. Demonstration of controller behavior

The similarities and differences between the controllers are visualized in Fig. 7 by presenting data from a single representative day.

BAU maintains the room temperatures at the lowest possible level to save energy while disregarding the current price signal. In contrast, the heat consumption of the buildings controlled by MPC and FLC is shifted to periods with low energy prices, indicated by strong heating and thus increasing room temperatures (e.g., between 00:00 and 06:00). However, while FLC uniformly preheats all rooms, MPC utilizes room-individual models and, therefore, controls each room differently. For instance, rooms R1 and R3 are small rooms with a large window area and, thus, greater heat losses than other rooms. This information is implicitly contained in the room models, and accordingly, the MPC preheats these rooms less pronouncedly to avoid large heat losses. Furthermore, the FLC only preheats to around 22 °C, while the MPC preheats much further, reaching 23.5 °C. At the end of the day, MPC and FLC preheat the building as they anticipate increased prices the following day. Notably, the MPC incurs the highest peak loads, potentially endangering thermal fairness in DHNs, which should be compensated by appropriate communication with the network operator.

For a more detailed analysis, Fig. 8 and Fig. 9 present the indoor air temperatures and room-level heat flows for rooms R2 and R4 across all controllers during experiment 2.

A distinct difference between FLC and MPC is the timing of the preheating. The FLC begins to preheat the building six hours before the lower temperature bound increases and prevents preheating beyond 22 °C. While this helps the FLC to avoid violations of the upper temperature bound, it also limits its savings potential. In contrast, the MPC considers the upper temperature bound when making control decisions. Consequently, for the rooms in which the upper temperature bound is lowered to 22 °C at night, the MPC schedules the heating such that temperatures do not exceed 22 °C at night but are raised higher as soon as the upper temperature bound is relaxed at 8 am (see Fig. 9). Consequently, the MPC can simultaneously satisfy temperature constraints and utilize the building's flexibility. Nonetheless, preheating is only cost-effective if the energy prices fluctuate sufficiently. On Jan. 02, the energy prices remain almost constant, making preheating economically disadvantageous as it increases the heat losses. Both FLC and MPC recognize this and, accordingly, track the lower temperature constraint to conserve energy and, thereby, cost (see Fig. 8 and Fig. 9).

The experimental results of experiment 4's first day (Jan. 10, 2025) are visualized in Fig. 10.

The window opening is clearly reflected in the sudden temperature drops, for instance, around 6 am. Consequently, all controllers increase the heating to restore the indoor air temperatures to a comfortable level once the windows are closed. The MPC's thermal model of the kitchen (see Eq. (4)) contains the information that the kitchen receives waste heat when the other rooms are heated. When the windows are

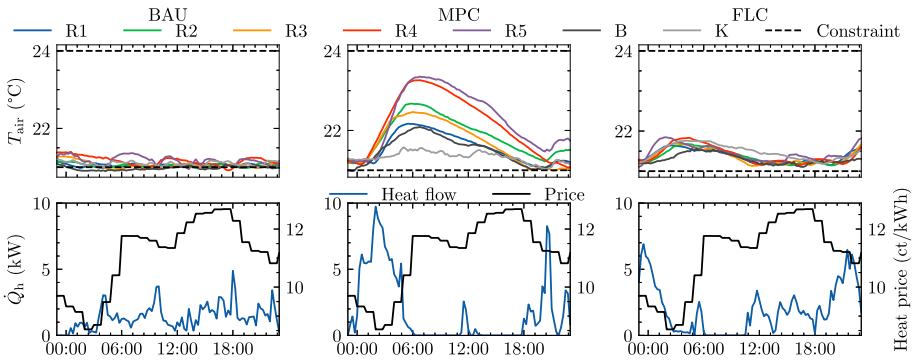

Fig. 7. Indoor air temperatures, total heat flow and price signal for each building on Dec. 22, 2024, during experiment 1.

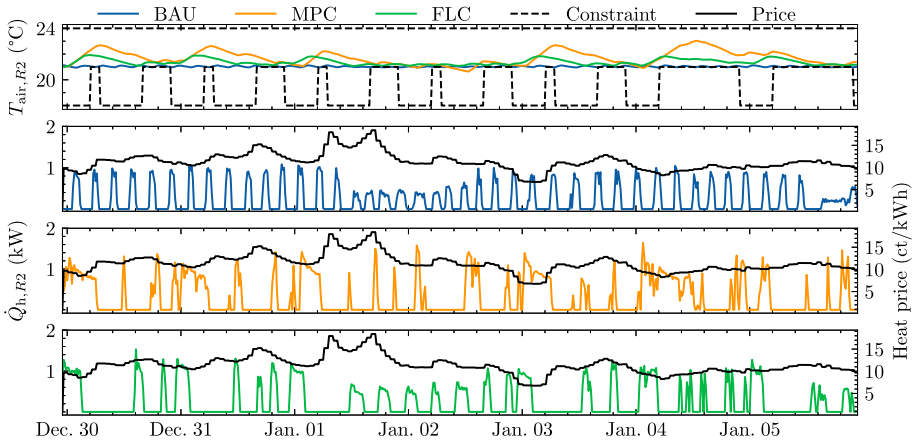

Fig. 8. Measured indoor air temperatures and heat flows in room R2 for all controls during experiment 2.

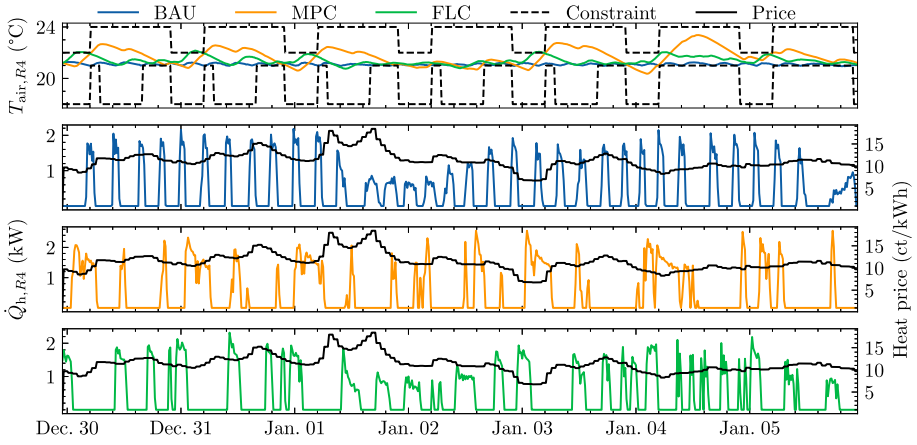

Fig. 9. Measured indoor air temperatures and heat flows in room R4 for all controls during experiment 2.

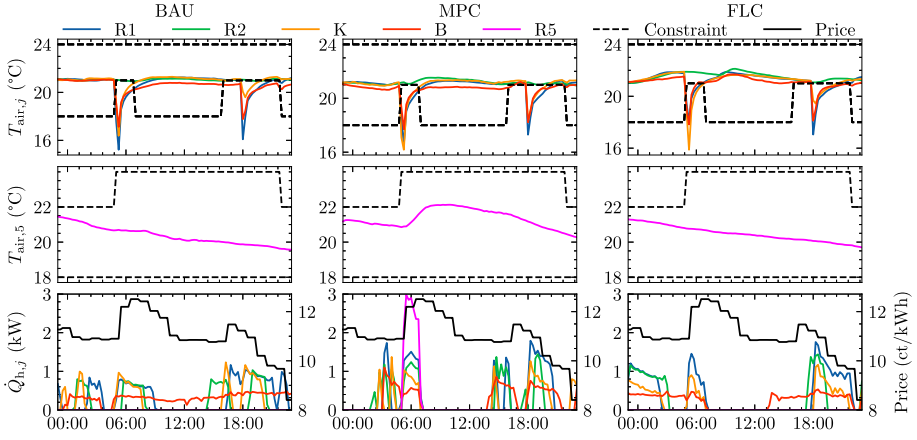

Fig. 10. Experimental results of Jan. 10, 2025, during experiment 4. Room R5 is visualized separately since it utilizes temperature bounds different from those of the other rooms.

opened, the temperature in the kitchen drops below the lower temperature bound, which is heavily penalized in the MPC's objective function (see Eq. (8)). Consequently, the MPC heats room R5 to utilize its waste heat in the kitchen, which is visible around 6 am as an increase in the temperature of R5. This behavior is technically optimal, considering the heavy penalization of temperature constraint violations. However, it is an undesirable artifact of the modeling approach, which has been removed for the remainder of experiment 4 by setting the fraction of waste heat of R5 to zero.

5.2. Cost and CO_2 savings

Fig. 11 depicts the savings of FLC and MPC with respect to BAU for all five experiments. While both control strategies consistently achieve

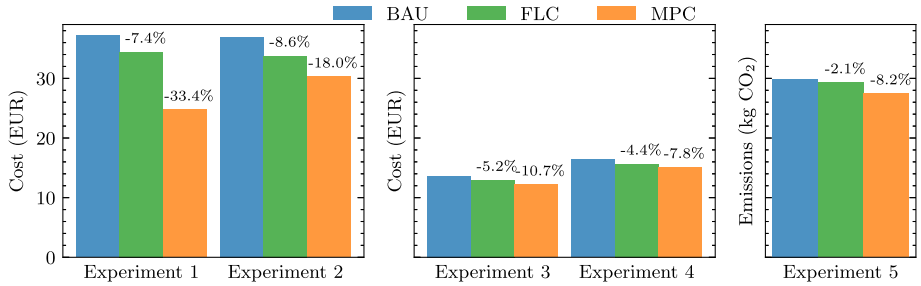

Fig. 11. Savings of FLC and MPC for all experiments. Experiments using the same price signals (see Table 2) are arranged in subplots.

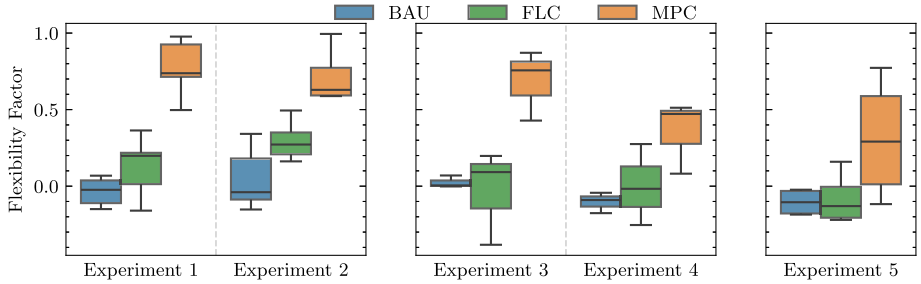

Fig. 12. Boxplots of the daily Flexibility Factors for all experiments and controls. Experiments using the same price signals are arranged in subplots.

cost/CO_2 savings in each experiment, the magnitude of the savings ranges from 2.1 % to 8.6 % for FLC and from 7.8 % to 33.4 % for MPC. The results of different experiments are not directly comparable because they ran for different durations (see Table 2) and due to varying weather conditions. Therefore, the focus is on comparing the controllers within each individual experiment. Nevertheless, the trend of declining savings from experiment 1 to experiment 4 is evident.

Considering experiments 1 and 2, two apparent differences between FLC and MPC exist. First, MPC achieves considerably higher savings of 33.4 % (≈12 EUR) compared to 7.4 % (≈3 EUR) in experiment 1 and 18 % (≈6 EUR) compared to 8.6 % (≈3 EUR) for experiment 2. Second, the savings of MPC decrease substantially from experiment 1 to experiment 2, while the FLC's remain stable. The differences are due to two distinct aspects between FLC and MPC: (i) the FLC only utilizes information about the current price in relation to the future prices without considering the absolute price value, and (ii) the FLC preheats the building at maximum to 22 °C, whereas the MPC is only limited by the upper temperature bound. Thereby, the MPC can save more cost by utilizing more of the building's flexibility by preheating it more pronouncedly. However, in experiment 2, the upper temperature bounds for rooms R3, R4, and R5 are lowered to 22 °C at night to prevent excessively high bedroom temperatures. This coincides with the times of low energy prices. Consequently, the usable flexibility of the building is reduced as the controllers cannot preheat these rooms further than 22 °C, ultimately decreasing the cost savings. However, since FLC does not preheat the building beyond 22 °C, it is barely affected, while MPC's cost savings are almost halved due to this reduced flexibility (see Fig. 11).

Both controllers achieve lower savings in experiments 3 and 4 than in experiments 1 and 2 since the underlying price signal shows less spread (see Fig. 6), which decreases the savings potential. The price spread refers to the price difference between low and high prices. Furthermore, temperature drops caused by window openings in experiment 4 force all controllers to increase heating to restore the indoor air temperature to comfortable levels regardless of the price. This further reduces the savings of FLC and MPC in experiment 4. Notably, in experiments 3 and 4, the performance difference between FLC and MPC is significantly lower than during experiments 1 and 2. This can be attributed to the MPC's lower preheating temperatures than in experiments 1 and 2 in response to the reduced spread of the price signal. Therefore, the behavior of FLC and MPC is more similar, reducing the performance difference.

Similarly, the savings for experiment 5 are lower than for experiments 1 and 2, as the CO_2 signal shows less spread than the "variable" price signal. However, the performance difference between FLC and MPC is larger than for experiments 3 and 4 since the same temperature constraints as in experiment 1 are applied (see Table 2), which offers more flexibility than the temperature constraints of experiments 2, 3, and 4, which the MPC can leverage through substantial preheating. In summary, both controllers consistently achieve savings in all experiments. While the MPC saves more cost, the achieved savings depend more on the flexibility potential, such as the price spread and the permitted temperature range. The success of the controllers in leveraging flexibility is evaluated using the Flexibility Factor.

5.3. Flexibility factor

Fig. 12 presents the daily FFs for all experiments and controls.

The FFs for BAU remain close to zero, indicating that BAU consumes as much heat during high-price periods as during low-price periods. This is to be expected, as BAU does not utilize price information. Conversely, the FFs for MPC and FLC are positive, indicating that both controls consume more heat during low than high-price times. Nonetheless, the FFs for MPC are substantially greater than those for FLC. Across all experiments, MPC achieves a median FF of 0.66, FLC of 0.17, and BAU of −0.04. In experiment 1, MPC achieves a median FF of 0.74 compared to a median FF of 0.20 for FLC. As discussed in Section 5.2, the tighter air temperature bounds imposed in experiment 2 reduce the flexibility potential, resulting in the more similar performance of FLC and MPC compared to experiment 1. This is also reflected in more similar FFs as MPC achieves a median FF of 0.63 and FLC of 0.27 in experiment 2. The same holds for experiment 4, where window openings force the controllers to heat during high-price periods to restore thermal comfort. This reduces the load shifting potential and, consequently, the FFs, which is particularly pronounced for MPC. Notably, under FLC, several days with negative FFs occur, indicating that more heat is consumed during periods with high prices than with low prices. In contrast, this only occurs for a single day under the MPC.

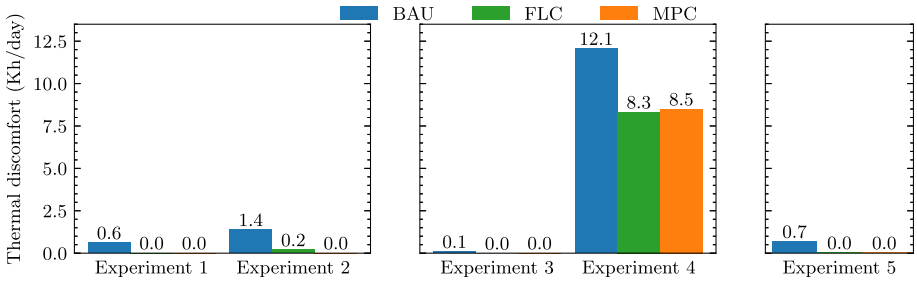

Fig. 13. Room-average daily thermal discomfort of BAU, FLC and MPC for all experiments. Experiments using the same price signals are arranged in subplots.

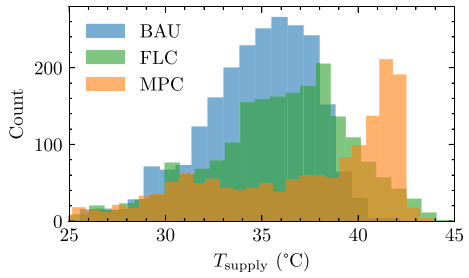

Fig. 14. Histograms of the measured supply temperatures for each controller across all experiments.

Both control strategies achieve their lowest FFs in experiment 5 when aiming to minimize CO_2 emissions. This is due to the more stable trend of the CO_2 signal compared to the price signals (see Fig. 6). For instance, on "Day 4", the CO_2 signal continuously declines throughout the day. Consequently, to achieve high values of the FF, heating has to be deferred to the end of the day, which is infeasible as thermal comfort must be ensured. In contrast, the price signal tends to decline or increase only for multiple hours but not entire days (see Fig. 6), whereby preheating can be used to avoid heating during high-price periods.

Solely focusing on cost savings and the FF does not provide a complete overview of the control performance since low costs can also be achieved by insufficient heating. Therefore, thermal discomfort also has to be considered.

5.4. Thermal discomfort

The thermal discomfort is quantified by the integrated and room-averaged lower and upper temperature bounds violations and is presented in Fig. 13 for all experiments and controllers.

Under the ideal conditions of experiments 1, 2, 3, and 5, both FLC and MPC almost completely eliminate thermal discomfort. In experiment 4, temperature constraint violations are inevitable as windows are opened. Nevertheless, the thermal discomfort experienced in buildings controlled by FLC and MPC is approximately 30 % lower than that of the BAU. This reduction is achieved as FLC and MPC increase the supply temperature to quickly restore the indoor air temperature to an acceptable level. In contrast, the supply temperature selected by BAU is bound to the heating curve. Fig. 14 visualizes the distributions of the different supply temperatures selected by the controllers.

Notably, MPC predominantly selects high supply temperatures, as it preheats the building at maximum capacity while the energy prices are low. Similarly, FLC also selects higher supply temperatures than BAU, as it computes a correction factor that increases the supply temperature obtained from the heating curve when energy prices are low or when heating is required.

While experiments 1–4 focused on cost minimization, which is essential to facilitate a widespread application of advanced control, the control should eventually also reduce greenhouse gas emissions. This is explored in experiment 5.

5.5. Comparison between cost and CO_2 minimization

Fig. 15 compares the experimental results of room R4 in the experiments 1 and 5 for the MPC.

While the price and CO_2 signals show similar trends, they do not consistently align. For instance, at the beginning of "Day 3", the price signal is low and increases during the day, while the CO_2 signal remains comparatively high and mostly stable during the day. Consequently, the controller selects different heating strategies by heating the building substantially at the beginning of "Day 3" for experiment 1, whereas in experiment 5, the heating is deferred to the afternoon. Notably, while the MPC achieves 33.4 % of cost savings in experiment 1, it only reduces the CO_2 emissions by 2.9 %. This highlights that solely prioritizing cost minimization fails to fully leverage the potential for reducing emissions.

5.6. Cost estimation of the control implementation

The costs for implementing the presented advanced controls comprise three parts: hardware, software, and labor.

Both the FLC and MPC were executed on desktop computers. The computer executing the FLC is equipped with an Intel Core i7-10700 K CPU@3.80 GHz and 32 GB RAM, while the computer running the MPC features an AMD Ryzen 9 5900X CPU@3.7 GHz and 64 GB RAM. Executing FLC and MPC involves reading the current room air temperatures, computing the new temperature setpoints, and writing these setpoints to the building. This process, which is repeated at every time step, takes approximately 15 s for the FLC and 60 s for the MPC.

Further, FLC and MPC require eight internet-connected indoor air temperature sensors (€110 each) and eleven actuators (€15 each) to adjust valve openings in the rooms. Additionally, one actuator is required to control the supply temperature (€100), along with a PLC to manage sensor and actuator communication (€1200).

MPC requires eleven additional heat flow meters to measure room-individual heat flows for model identification (€330 each). However, as these are only necessary for model identification and not during regular operation, reusable clamp-on heat flow meters can be utilized. When deploying advanced control at scale, the cost per building for these reusable meters decreases significantly. Alternatively, heat-measurement-free model identification methods can also reduce implementation costs [45].

Regarding software implementation, MATLAB has been used for model identification, and Python for control development and execution. Data storage is facilitated through InfluxDB, and communication with actuators is managed via MQTT. While a MATLAB license for non-academic use currently costs €2345, it can easily be replaced with the free, open-source programming language Python. Furthermore, accessing the weather forecasts from the German Weather Service via an application programming interface is free of charge [36].

The hardware and software setup used in the present study is provided by a research building that is well-equipped with numerous

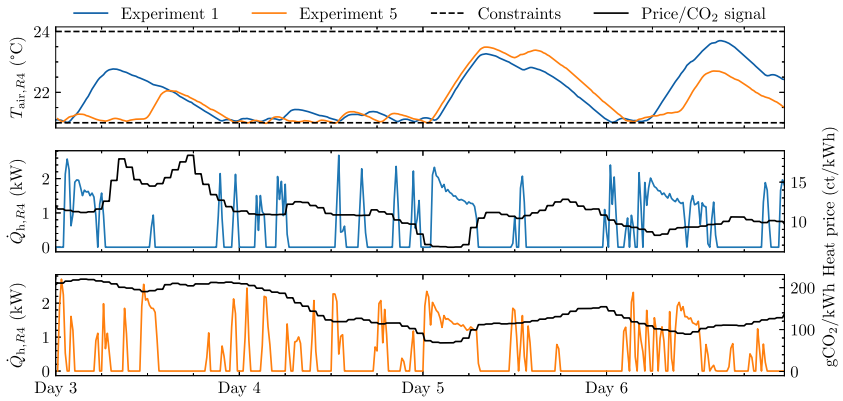

Fig. 15. Comparison of cost minimization (experiment 1) and CO_2 minimization (experiment 5) for the MPC in room R4.

sensors for detailed validation of the developed control strategies. When retrofitting a residential building, utilizing smart thermostats is a more cost-effective approach. These thermostats can measure the room air temperature, track temperature setpoints, store the collected data, and offer an application programming interface for communication. This considerably reduces the implementation requirements by eliminating the need for additional indoor air temperature sensors, valve actuators, InfluxDB, MQTT, and the PLC.

The development and deployment of the FLC and MPC required approximately 125 person-days of labor. This includes 55 person-days of preparation, which involved sensor validation, concept development, and creating and interfacing databases. Additionally, 20 person-days were spent on model identification (just for MPC), 40 days on developing the controller software (for FLC and MPC), and 10 days on deploying and tuning the controllers (for FLC and MPC). Notably, the building was already equipped with sensors, actuators, and a communication interface, which reduced labor requirements. We expect that future implementations of advanced building controls will require significantly less time, as the developed software can be largely reused.

6. Conclusion

The present work compares fuzzy logic control (FLC) and model predictive control (MPC) against a baseline (baseline-as-usual (BAU)) in a four-week experimental study. By controlling three architecturally identical buildings in a real-world experiment, each with a different controller, the controllers' performances can be directly evaluated under nearly identical conditions. Three metrics are selected to evaluate the control performance: the Flexibility Factor (FF), heating costs, and thermal discomfort. The controls aim to minimize heating costs and CO_2 emissions in response to dynamic pricing. Various experiments are conducted, encompassing different price signals, comfort bounds, and emulated occupant behavior.

The findings show that both FLC and MPC can activate their buildings' energy flexibility to shift heat demand from high-price periods to low-price periods, as indicated by higher values of the FF compared to the benchmark. However, the FFs are substantially greater for MPC than for FLC, with median FFs of 0.63 and 0.17, respectively. Consequently, the MPC can utilize the buildings' flexibility potential to a larger extent. When minimizing CO_2 emissions, both controllers obtain lower FFs than when minimizing heating costs. This is attributed to the more stable trends of the CO_2 signal compared to the price signals. By successfully using the buildings' energy flexibility, FLC and MPC consistently save heating costs across all experiments. Specifically, cost savings for MPC range from 7.8 % to 33.4 % and for FLC from 4.4 % to 8.6 %. In addition, both control strategies achieve comparable and substantial improvements in maintaining a comfortable indoor air temperature.

Although MPC realizes greater cost savings, it strongly depends on the existing flexibility potential, such as the price spread and the permitted temperature range for the indoor air temperature. In particular, in experiments with low price spreads, the additional savings offered by MPC over FLC do not appear to justify the increased implementation complexity. In contrast, the MPC achieves substantially greater savings in experiments characterized by either high price spreads or high flexibility potentials. Consequently, investing in MPC is advantageous in markets with high price spreads and in applications with substantial flexibility potential.

Increasing the share of renewable electricity generation reduces both the spot market price of electricity [46] and the CO_2 emissions per unit of electricity generated [47], compared to fossil fuel generation. However, when minimizing cost, the MPC reduces CO_2 emissions by only 2.9 % while saving 33.4 % of costs. Consequently, focusing solely on cost minimization is insufficient to achieve substantial emission reductions.

In the present study, the heat pump supplying the district heating network is modeled with a constant efficiency. If the efficiency were to vary, the controllers would need to balance thermal comfort, energy costs, and heat pump efficiency. Varying efficiency would likely increase price variability and, consequently, the differences between the MPC and FLC.

The FLC applied in this work does not raise the indoor air temperatures beyond 22 °C. While this prevents the controller from compromising thermal comfort by overheating, it also limits the flexibility potential and, thereby, the achievable savings. Future work will explore modifying the FLC to maximize flexibility while ensuring thermal comfort. Further, the present work focuses on accurately comparing the performance of various controllers for individual buildings, emphasizing the achievable savings. While savings are central to encouraging consumers to adopt new technologies, uncoordinated responses to dynamic prices can stress the electricity grid [48] when employing electric heating systems or could jeopardize thermal fairness in district heating networks. Consequently, future work will develop and evaluate control strategies that manage the experimental buildings while coordinating them to account for grid constraints.

CRediT authorship contribution statement

Felix Langner: Writing – original draft, Visualization, Software, Project administration, Methodology, Investigation, Formal analysis, Data curation, Conceptualization. **Jovana Kovačević:** Writing – original draft, Visualization, Software, Methodology, Investigation, Formal analysis, Data curation, Conceptualization. **Luigi Spatafora:** Writing – review & editing, Resources, Formal analysis, Data curation, Conceptualization. **Stefan Dietze:** Writing – review & editing, Software, Formal analysis, Data curation, Conceptualization. **Simon Waczowicz:** Writing – review & editing, Resources, Funding acquisition,

Conceptualization. **Hüseyin K. Çakmak:** Writing – review & editing, Supervision, Resources, Funding acquisition, Conceptualization. **Jörg Matthes:** Writing – review & editing, Supervision, Resources, Funding acquisition, Conceptualization. **Veit Hagenmeyer:** Writing – review & editing, Supervision, Resources, Funding acquisition, Conceptualization.

Declaration of generative AI and AI-assisted technologies in the writing process

During the preparation of this work the authors used Microsoft Copilot in order to improve the readability and language of the manuscript. After using this tool, the authors reviewed and edited the content as needed and take full responsibility for the content of the publication.

Declaration of competing interest

The authors declare that they have no known competing financial interests or personal relationships that could have appeared to influence the work reported in this paper.

Acknowledgments

We acknowledge the financial support of the Helmholtz Association of German Research Centres (HGF) within the framework of the Program-Oriented Funding POF IV in the program Energy System Design (ESD, project numbers 37.12.01, 37.12.02, and 37.12.03).

Appendix A. FLC design

All input and output membership functions are depicted in Fig. A.16, where μ represents the degree of the membership of the corresponding input value. The inputs are presented in plots Fig. A.16 (a) – (d) and the outputs in (e) and (f). The change of the lower temperature bound Fig. A.16(c) is presented with three triangular membership functions, as the lower temperature bounds $\underline{T}$ differ only between 18 °C and 21 °C (i.e., ± 3 K). Membership functions of the control signal $\Delta T_{\text{supply},j}$, depicted in Fig. A.16(f), have only positive output values since the baseline supplied water temperature is only increased if necessary for achieving the next set-point temperature $T^{\text{set}}_{\text{air},j}$. In Fig. A.16(e), T_{off} is not presented but is utilized when the room is not occupied, i.e., $\underline{T}_j = 18$ °C and is defined as a triangular function between 17.5 °C and 18.5 °C with a peak at 18 °C, without the intersection with the rest of the membership functions.

Fig. A.17 depicts the control signals $T^{\text{set}}_{\text{air},j,k+1}$ and $\Delta T_{\text{supply},j,k+1}$ for the case when $\underline{T}_j = 21$ °C, $e_{j,k} = 0$, and $\Delta o_{j,k} = 0$ while the rest of the inputs vary. On the axis where $\Delta T_{\text{air},j}$ changes, the steep slope can be observed, which means that both control signals are quickly increased as soon as the negative disturbance (e.g., window opening) occurs. Furthermore, it can be noticed that when $\hat{F}(p_{\text{buy}})_k$ is high, both control signals are kept low for the sake of cost minimization.

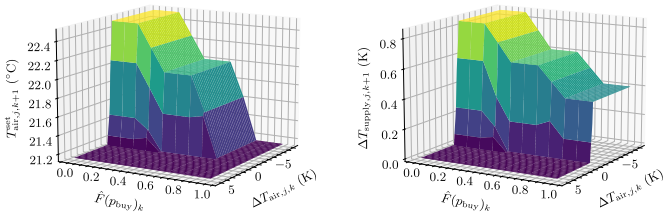

Fig. A.17. The FLC graph depicts the dependence of subsequent control signals on two inputs: the ECDF of the price and the change of temperature. The case of $\underline{T}_{j,k} = 21$ °C is depicted. The remaining two input signals are kept constant $e_{j,k} = 0$ K and $\Delta o_{\text{j,k}} = 0$ K.

Appendix B. Data collection and model validation

Since the experimental buildings are used as office buildings during the week, the weekends were used to develop the control algorithms without disturbing the office staff. From Oct. 12, 2024, until Dec. 15, 2024, each of the ten weekends was used to interact with the buildings to either (i) test the communication interfaces, (ii) verify the sensor readings, (iii) excite the buildings' heating systems with pseudo-random-binary-sequences to gather high-quality measurement data for the model identification, or (iv) evaluate the performance of preliminary versions of the control algorithms.

The models were trained on the data of four weekends (Nov. 9–10, 16–17, 23–24, and Dec. 1–2) and then validated on the data of the two following weekends, Dec. 7–8 and Dec. 14–15. Table B.6 presents each room's root mean square error (RMSE) values on both weekends used for validation.

Table B.6
Model validation results for each room on two weekends.

Rooms	RMSE Dec. 7–8, 2024 (K)	RMSE Dec. 14–15, 2024 (K)
R1	0.11	–
R2	0.07	0.11
R3	0.08	0.10
R4	0.06	0.09
R5	0.35	0.15
K	0.14	0.26
C	0.05	0.16
B	0.04	0.06

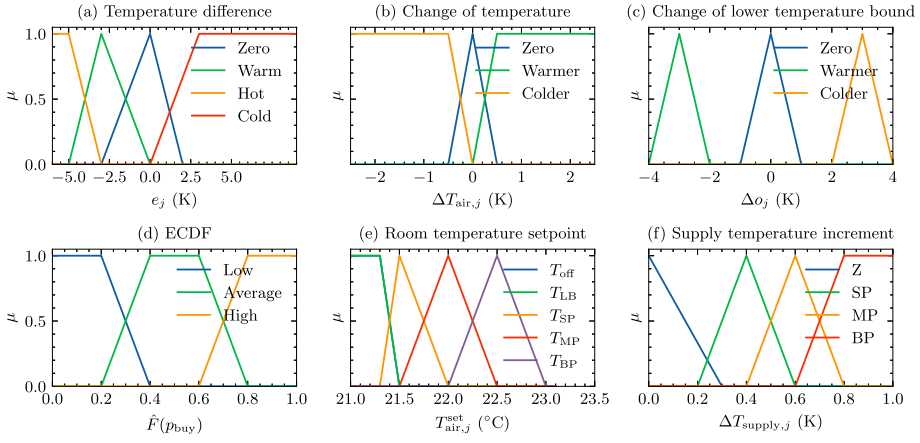

Fig. A.16. Membership functions for all inputs and outputs of FLC.

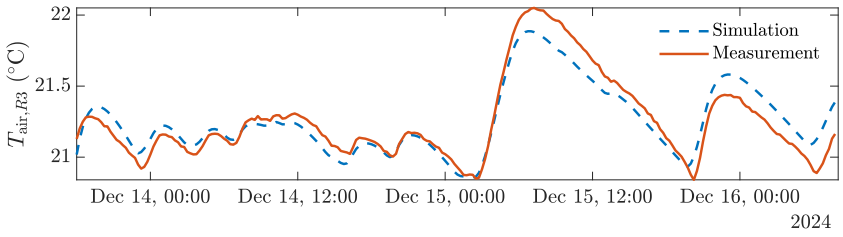

(a) Validation results of room R3 during Dec. 14 – 16, 2024.

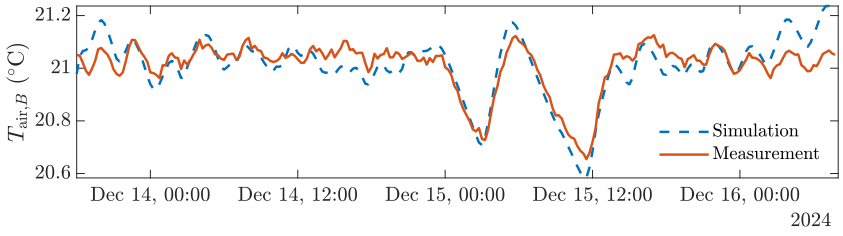

(b) Validation results of room B during Dec. 14 – 16, 2024.

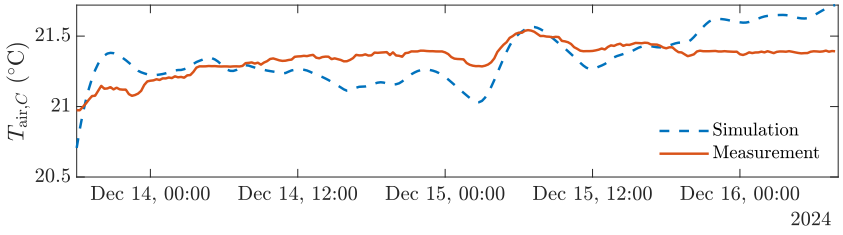

(c) Validation results of room C during Dec. 14 – 16, 2024.

Fig. B.18. Exemplary validation results of three rooms during one validation period.

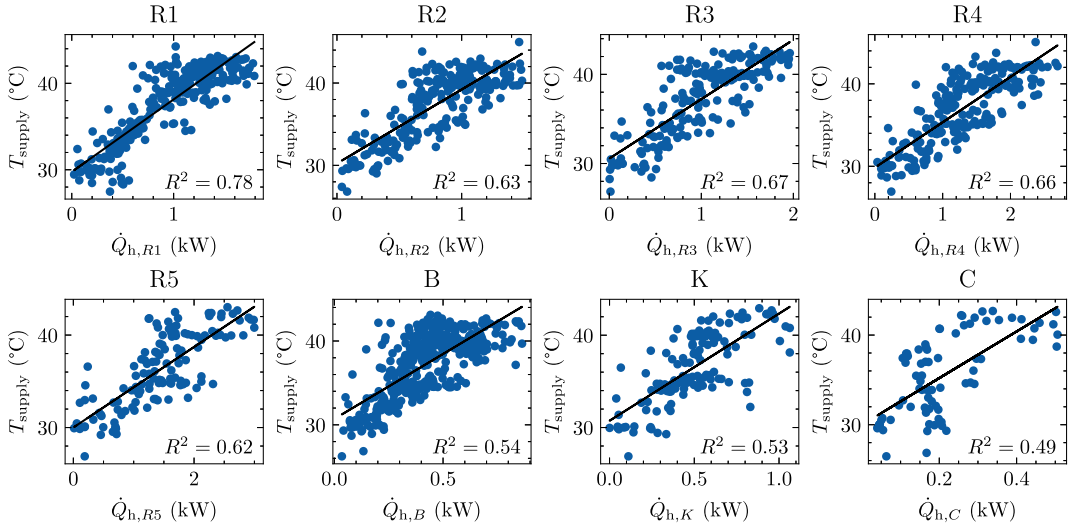

Fig. B.19. Linear functions mapping the heat flows to the supply temperature of the underfloor heating system.

All RMSE values are clearly below 1 K, indicating a sufficiently accurate model fit. No reliable RMSE can be reported for the validation of R1 on Dec. 14–15, as the window in R1 was accidentally left partially open, thereby substantially distorting the temperature measurements. Before the start of the experiments, the models were retrained on all available data, including the validation period, to incorporate all information into the final model. Fig. B.18 presents the validation results of rooms R3, B, and C on Dec. 14–15, 2024, which represent average, above average, and below average model identification results.

The parameter identification for rooms K and C obtains similar RMSE values to those of the other rooms. However, the temperature dynamics in K and C are not as accurately captured as visible in Fig. B.18a. The reason for this is that the parameter estimation for K and C is impacted by the substantial waste heat received from the heating of the other rooms (see Eq. (4)).

Besides the models describing the rooms' thermal behavior, the MPC also requires a model to map the rooms' heat flows to a supply temperature of the underfloor heating system. As discussed in Section 3.3, linear regression has been found to be sufficiently accurate. Fig. B.19 presents the resulting models, where the black lines are the identified linear functions m_j mapping heat flows to supply temperatures.

Table C.7
The disturbance schedule. D: doors, W: windows, R: roller shutters, o: open, c: closed.

Time	R1			R2			R3			R4			R5			K			C		B		
	D	W	R	D	W	R	D	W	R	D	W	R	D	W	R	D	W	R	W	R	D	W	R
06:00	c	c	o	c	c	o	c	c	o	c	c	o	c	c	o	c	c	o	c	o	c	c	o
06:05	o	o	o	c	c	o	c	c	o	o	o	o	c	c	o	o	o	o	o	o	o	o	o
06:15	o	c	o	c	c	o	c	c	o	o	c	o	c	c	o	o	c	o	c	o	o	c	o
19:00	o	o	o	c	c	o	c	c	o	o	c	o	c	c	o	o	o	o	c	o	o	c	o
19:10	o	c	o	c	c	o	c	c	o	o	c	o	c	c	o	o	c	o	c	o	o	c	o
22:45	o	c	o	c	c	o	c	c	o	o	o	o	c	c	o	o	c	o	c	o	o	c	o
22:55	o	c	o	c	c	o	c	c	o	o	c	o	c	c	o	o	c	o	c	o	o	c	o
23:00	c	c	c	c	c	c	c	c	c	c	c	c	c	c	o	c	c	o	c	o	c	c	o

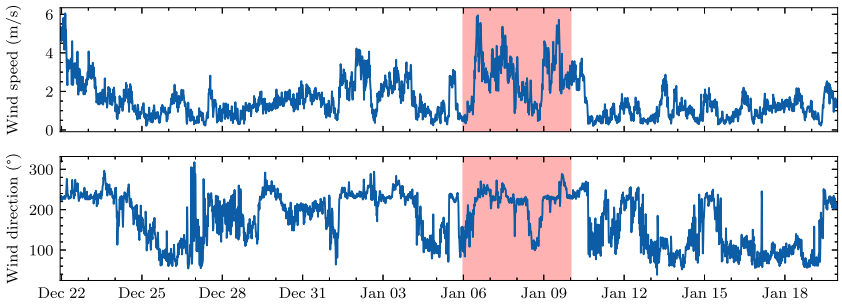

Fig. D.20. Wind speed and direction throughout the experimental period.

Appendix C. Disturbance schedule

The disturbance schedule mimics occupant behavior and is presented in Table C.7. The inner doors, roller shutters, and windows are closed at night. At 6 am, the roller shutters are opened, and at 6:05 am, the inner doors and windows are opened to ventilate the buildings for ten minutes. In the evening, the kitchen (K) and dining room (R1) are ventilated for ten minutes again. Before bedtime, the children's room (R4) is also ventilated for ten minutes.

Appendix D. Wind measurements

Fig. D.20 presents the wind speed and direction throughout the experimental period. The wind directions north, east, south, and west correspond to 0 °C, 90 °C, 180 °C, and 270 °C, respectively. The scenario "Energy comparison" is highlighted in red. Notably, during this time, the wind speeds were significantly higher than during the remaining time and mostly occurred from the western direction. This most probably led to the lower energy consumption of Building 3 compared to Buildings 1 and 2 (see Fig. 1a) during the experiment "Energy comparison".

Data availability

Data will be made available upon request.

References

[1] International Energy Agency. Buildings. https://www.iea.org/energy-system/buildings. [accessed: 2025-Feb-25].
[2] IEA. Transition to sustainable buildings; 2013, https://www.iea.org/reports/transition-to-sustainable-buildings. [accessed: 2025-Feb-25].
[3] Lund H, Østergaard PA, Nielsen TB, Werner S, Thorsen JE, Gudmundsson O, et al. Perspectives on fourth and fifth generation district heating. Energy 2021;227:120520. https://doi.org/10.1016/j.energy.2021.120520
[4] Novosel T, Feijoo F, Duić N, Domac J. Impact of district heating and cooling on the potential for the integration of variable renewable energy sources in mild and Mediterranean climates. Energy Convers Manag 2022;272:116374. https://doi.org/10.1016/j.enconman.2022.116374
[5] Kohlhepp P, Gröll L, Hagenmeyer V. Characterization of aggregated building heating, ventilation, and air conditioning load as a flexibility service using gray-box modeling. Energy Technol 2021;9(9):2100251. https://doi.org/10.1002/ente.202100251
[6] Kohlhepp P, Harb H, Wolisz H, Waczowicz S, Müller D, Hagenmeyer V. Large-scale grid integration of residential thermal energy storages as demand-side flexibility resource: a review of international field studies. Renew Sustain Energy Rev 2019;101:527–47. https://doi.org/10.1016/j.rser.2018.09.045
[7] Kohlhepp P, Hagenmeyer V. Technical potential of buildings in Germany as flexible power-to-heat storage for smart-grid operation. Energy Technol 2017;5(7):1084–104. https://doi.org/10.1002/ente.201600655
[8] David A, Mathiesen BV, Averfalk H, Werner S, Lund H. Heat roadmap Europe: large-scale electric heat pumps in district heating systems. Energies 2017;10(4):578. https://doi.org/10.3390/en10040578
[9] Siano P. Demand response and smart grids—a survey. Renew Sustain Energy Rev 2014;30:461–78. https://doi.org/10.1016/j.rser.2013.10.022
[10] Vandermeulen A, van der Heijde B, Helsen L. Controlling district heating and cooling networks to unlock flexibility: a review. Energy 2018;151:103–15. https://doi.org/10.1016/j.energy.2018.03.034
[11] Foteinaki K, Li R, Péan T, Rode C, Salom J. Evaluation of energy flexibility of low-energy residential buildings connected to district heating. Energy Build 2020;213:109804. https://doi.org/10.1016/j.enbuild.2020.109804
[12] Le Dréau J, Lopes RA, O'Connell S, Finn D, Hu M, Queiroz H, et al. Developing energy flexibility in clusters of buildings: a critical analysis of barriers from planning to operation. Energy Build 2023;300:113608. https://doi.org/10.1016/j.enbuild.2023.113608
[13] Péan TQ, Salom J, Costa-Castelló R. Review of control strategies for improving the energy flexibility provided by heat pump systems in buildings. J Process Control 2019;74:35–49. https://doi.org/10.1016/j.jprocont.2018.03.006
[14] Frahm M, Dengiz T, Zwickel P, Maaß H, Matthes J, Hagenmeyer V. Occupant-oriented demand response with multi-zone thermal building control. Appl Energy 2023;347:121454. https://doi.org/10.1016/j.apenergy.2023.121454. https://linkinghub.elsevier.com/retrieve/pii/S0306261923008188
[15] Clauß J, Stinner S, Sartori I, Georges L. Predictive rule-based control to activate the energy flexibility of Norwegian residential buildings: case of an air-source heat pump and direct electric heating. Appl Energy 2019;237:500–18. https://doi.org/10.1016/j.apenergy.2018.12.074
[16] Mishra AK, Jokisalo J, Kosonen R, Kinnunen T, Ekkerhaugen M, Ihasalo H, et al. Demand response events in district heating: results from field tests in a university building. Sustain Cities Soc 2019;47:101481. https://doi.org/10.1016/j.scs.2019.101481
[17] Keshtkar A, Arzanpour S, Keshtkar F, Ahmadi P. smart residential load reduction via fuzzy logic, wireless sensors, and smart grid incentives. Energy Build 2015;104:165–80. https://doi.org/10.1016/j.enbuild.2015.06.068
[18] Talebi A, Hatami A. Online fuzzy control of HVAC systems considering demand response and users' comfort. Energy Sources Part B Econ Plan Policy 2020;15(7–9):403–22. https://doi.org/10.1080/15567249.2020.1825557
[19] Knudsen MD, Georges L, Skeie KS, Petersen S. Experimental test of a black-box economic model predictive control for residential space heating. Appl Energy 2021;298:117227. https://doi.org/10.1016/j.apenergy.2021.117227
[20] Thorsteinsson S, Kalaee AAS, Vogler-Finck P, Stærmose HL, Katic I, Bendtsen JD. Long-term experimental study of price responsive predictive control in a real occupied single-family house with heat pump. Appl Energy 2023;347:121398. https://doi.org/10.1016/j.apenergy.2023.121398

[21] Hu M, Xiao F, Jørgensen JB, Li R. Price-responsive model predictive control of floor heating systems for demand response using building thermal mass. Appl Therm Eng 2019;153:316–29. https://doi.org/10.1016/j.applthermaleng.2019.02.107
[22] Wei Z, Calautit J. Investigation of the effect of the envelope on building thermal storage performance under model predictive control by dynamic pricing. Smart Energy 2022;6:100068. https://doi.org/10.1016/j.segy.2022.100068
[23] Ramesh R, Rehman HU, Hasan A, Eerolainen L, Yin H, Hamdy M. Optimising energy flexibility in Finnish residential buildings: a comparative study of PI, rule-based and model predictive control strategies. Energy Build 2025;338:115727. https://doi.org/10.1016/j.enbuild.2025.115727
[24] Wang C, Wang B, You F. Demand response for residential buildings using hierarchical nonlinear model predictive control for plug-and-play. Appl Energy 2024;369:123581. https://doi.org/10.1016/j.apenergy.2024.123581
[25] Morovat N, Athienitis AK, Candanedo JA, Nouanegue HF. Heuristic model predictive control implementation to activate energy flexibility in a fully electric school building. Energy 2024;296:131126. https://doi.org/10.1016/j.energy.2024.131126
[26] Hua P, Wang H, Xie Z, Lahdelma R. Integrated demand response method for heating multiple rooms based on fuzzy logic considering dynamic price. Energy 2024;307:132577.
[27] Henze GP, Kircher KJ, Braun JE. Why has advanced commercial HVAC control not yet achieved its promise? J Build Perform Simul 2024;18(2):1–12. https://doi.org/10.1080/19401493.2024.2429728
[28] Pergantis EN, Priyadarshan, Theeb NA, Dhillon P, Ore JP, Ziviani D, Groll EA, et al. Field demonstration of predictive heating control for an all-electric house in a cold climate. Appl Energy 2024;360:122820. https://doi.org/10.1016/j.apenergy.2024.122820
[29] Drgoňa J, Arroyo J, Cupeiro Figueroa I, Blum D, Arendt K, Kim D, et al. All you need to know about model predictive control for buildings. Annu Rev Control 2020;50:190–232. https://doi.org/10.1016/j.arcontrol.2020.09.001
[30] Hagenmeyer V, Kemal Çakmak H, Düpmeier C, Faulwasser T, Isele J, Keller HB, et al. Information and communication technology in Energy Lab 2.0: smart energies system simulation and control center with an open-street-map-based power flow simulation example. Energy Technol 2016;4(1):145–62. https://doi.org/10.1002/ente.201500304
[31] Wiegel F, Wachter J, Kyesswa M, Mikut R, Waczowicz S, Hagenmeyer V. smart Energy System Control Laboratory – a fully-automated and user-oriented research infrastructure for controlling and operating smart energy systems. at Automatisierungstech 2022;70(12):1116–33. https://doi.org/10.1515/auto-2022-0018
[32] Wang D, Chen Y, Wang W, Gao C, Wang Z. Field test of model predictive control in residential buildings for utility cost savings. Energy Build 2023;288:113026. https://doi.org/10.1016/j.enbuild.2023.113026
[33] Tajalli-Ardekani E, Langner F, Kovačević J, Spatafora L, Dietze S, Waczowicz S, et al. Experimental data of three identical residential buildings controlled with different controllers for heating demand response. 2025. https://doi.org/10.5281/zenodo.16259041
[34] Federal Ministry for Economic Affairs and Climate Action. Energieeinsparverordnung. https://www.bmwk.de/Redaktion/DE/Gesetze/Energie/EnEV.html
[35] German weather service [accessed: 2025-Feb-6, https://www.dwd.de/EN/Home/home_node.html
[36] Gutzmann B, Motl A. Wetterdienst. 2025. https://doi.org/10.5281/zenodo.15579924
[37] Smart energy tariff|tado°. https://www.tado.com/en/energy/smart-energy-tariff. [accessed: 2025-Feb-20]
[38] Bundesnetzagentur. Festlegung von netzentgelten für steuerbare anschlüsse und verbrauchseinrichtungen. https://www.bundesnetzagentur.de/DE/Beschlusskammern/BK08/BK8_06_Netzentgelte/68_Para14a_EnWG/BK8_14a_EnWG.html. [accessed: 2025-Apr-11].
[39] Zahlen, Daten und Fakten zur Fernwärme in Karlsruhe. https://www.stadtwerke-karlsruhe.de/de/pk/fernwaerme/zahlen-und-preise.php. [accessed: 2025-Feb-20]
[40] Bundesnetzagentur. SMARD Strommarktdaten. https://www.smard.de/home/downloadcenter/download-marktdaten. [accessed: 2025-Feb-20].
[41] IPCC. AR5 synthesis report: Climate Change 2014 — IPCC; 2014. https://www.ipcc.ch/report/ar5/syr/. [accessed: 2025-Feb-28].
[42] MVV Energie AG. MVV flusswärmepumpe Mannheim. https://www.mvv.de/ueber-uns/unternehmensgruppe/mvv-umwelt/aktuelle-projekte/mvv-flusswaermepumpe?category=0&question=1987. [accessed: 2025-Feb-7].
[43] Ueno T, Meier A. A method to generate heating and cooling schedules based on data from connected thermostats. Energy Build 2020;228:110423. https://doi.org/10.1016/j.enbuild.2020.110423
[44] Le Dréau J, Heiselberg P. Energy flexibility of residential buildings using short term heat storage in the thermal mass. Energy 2016;111:991–1002. https://doi.org/10.1016/j.energy.2016.05.076
[45] Knudsen MD, Fiorentini M, Petersen S. A heat-measurement-free strategy for economic model predictive control of hydronic radiators. J Build Eng 2024;97:110694. https://doi.org/10.1016/j.jobe.2024.110694
[46] Sensfuß F, Ragwitz M, Genoese M. The merit-order effect: a detailed analysis of the price effect of renewable electricity generation on spot market prices in Germany. Energy Policy 2008;36(8):3086–94. https://doi.org/10.1016/j.enpol.2008.03.035
[47] Van Den Bergh K, Delarue E, D'Haeseleer W. Impact of renewables deployment on the Co_2 price and the Co_2 emissions in the European electricity sector. Energy Policy 2013;63:1021–31. https://doi.org/10.1016/j.enpol.2013.09.003
[48] Shen L, Li Z, Sun Y. Performance evaluation of conventional demand response at building-group-level under different electricity pricings. Energy Build 2016;128:143–54. https://doi.org/10.1016/j.enbuild.2016.06.082